JACS
JOURNAL OF THE AMERICAN CHEMICAL SOCIETY

Article

pubs.acs.org/JACS

Optical Imaging of Phase Transition and Li-Ion Diffusion Kinetics of Single $LiCoO_2$ Nanoparticles During Electrochemical Cycling

Dan Jiang,[†] Yingyan Jiang,[†] Zhimin Li,[†] Tao Liu,[†] Xiang Wo,[†] Yimin Fang,[†] Nongjian Tao,[†,‡] Wei Wang,[*,†] and Hong-Yuan Chen[†]

[†]School of Chemistry and Chemical Engineering, State Key Laboratory of Analytical Chemistry for Life Science, Nanjing University, Nanjing 210093, China

[‡]Center for Bioelectronics and Biosensors, Biodesign Institute, Arizona State University, Tempe, Arizona 85287, United States

Supporting Information

ABSTRACT: Understanding the phase transition and Li-ion diffusion kinetics of Li-ion storage nanomaterials holds promising keys to further improve the cycle life and charge rate of the Li-ion battery. Traditional electrochemical studies were often based on a bulk electrode consisting of billions of electroactive nanoparticles, which washed out the intrinsic heterogeneity among individuals. Here, we employ optical microscopy, termed surface plasmon resonance microscopy (SPRM), to image electrochemical current of single $LiCoO_2$ nanoparticles down to 50 fA during electrochemical cycling, from which the phase transition and Li-ion diffusion kinetics can be quantitatively resolved in a single nanoparticle, in operando and high throughput manner. SPRM maps the refractive index (RI) of single $LiCoO_2$ nanoparticles, which significantly decreases with the gradual extraction of Li-ions, enabling the optical read-out of single nanoparticle electrochemistry. Further scanning electron microscopy characterization of the same batch of nanoparticles led to a bottom-up strategy for studying the structure−activity relationship. As RI is an intrinsic property of any material, the present approach is anticipated to be applicable for versatile kinds of anode and cathode materials, and to facilitate the rational design and optimization toward durable and fast-charging electrode materials.

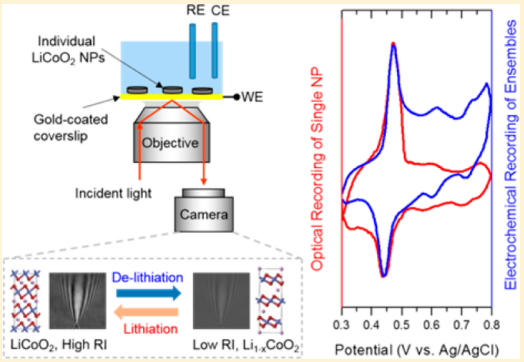

INTRODUCTION

Li-ion battery has been a major format of power supplies in portable devices and electric vehicles. Understanding the phase transition and Li-ion diffusion kinetics in the anode and cathode materials is critical to address the deformation and stress issues, which are some of the most significant challenges for their applications.[1] For instance, the utilization of nanosized Li-ion storage materials in the positive and negative electrodes has significantly improved the charge rate and cycle life of Li-ion batteries,[2−4] because the reduction of material dimensions not only accelerates the Li-ion diffusion, but also decreases the stress produced during the phase transition. Because of the intrinsic heterogeneity among individual nanoparticles, studying the phase transition and Li-ion diffusion kinetics at the single nanoparticle level represents an efficient way to understand the microscopic mechanism[5,6] and to establish the structure−activity relationship, which eventually helps the rational design and optimization of durable and fast-charging electrode materials.

Imaging the phase transition and Li-ion diffusion kinetics at the single nanoparticle level is a challenging task. Traditional electrochemistry techniques often measured the current of bulk electrode during electrochemical cycling, from which the averaged insertion and extraction kinetics of all Li-ions in the bulk electrode were determined. Such apparent kinetics not only reflected the intrinsic Li-ion migration behaviors within the nanoparticle lattice. It was also largely affected by the interparticle junctions and boundaries depending on the fabrication process, thus hampering the clarification of the crystallographic structure−activity relationship. For this reason, in situ imaging techniques, such as transmission electron microscopy (TEM)[5,7,8] and X-ray transmission microscopy,[6,9] have recently emerged as powerful tools to visualize the lithiation kinetics at the single nanoparticle level. While their outstanding spatial resolution is mostly suitable for monitoring the evolution of atomic structures, the temporal resolution was often not good enough to resolve the fast Li-ion diffusion kinetics at the subsecond time scale, especially for cathode materials whose morphological changes were usually subtle. In addition, high energy electron beams or X-rays could introduce additional uncertainties to the electrochemical reactions in the presence of electrolyte and solvent.

Optical microscopy[10−12] exhibits several features that are suitable for in situ imaging the electrochemical reactions of single nanoparticles, including high temporal resolution, noninvasiveness, high throughput, and low cost. It is routine for optical microscopes to simultaneously image lots of

Received: August 25, 2016
Published: December 13, 2016

DOI: 10.1021/jacs.6b08923
J. Am. Chem. Soc. 2017, 139, 186−192

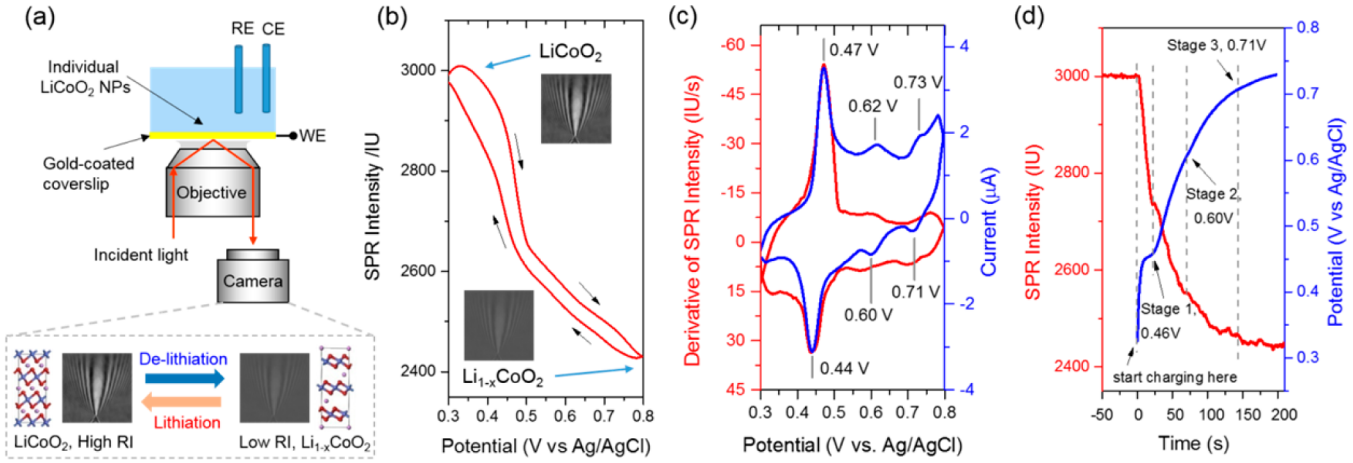

Figure 1. (a) Schematic illustration of monitoring the electrochemical lithiation of single $LiCoO_2$ nanoparticles. Delithiation decreases the refractive index (RI) of an individual nanoparticle, leading to a decreased optical contrast in the SPRM image. (b) SPR intensity curve of a single $LiCoO_2$ nanoparticle with application of a cyclic voltammetry sweep between 0.3 and 0.8 V. (c) The first order derivative of the SPR intensity curve (red curve) represents the cyclic voltammogram of a single nanoparticle, which is in good agreement with the averaged electrochemical current contributed by all $LiCoO_2$ nanoparticles on the gold film (blue curve). Note that the charging current is significantly reduced in the red curve (see Supporting Information section 2 for details). (d) SPR intensity of a single $LiCoO_2$ nanoparticle when applying a constant-current charging (red curve). The bulk electrode potential is shown as the blue curve. Charging starts at time zero.

individual nanoparticles with a temporal resolution of submilliseconds. Visible light illumination introduces minimal disturbance to the reaction medium, and it does not require an expensive instrument or synchrotron facility. Recently, bright-field optical microscopy was used to study the Li-ion intercalation in a large layer of graphite based on the increased transparency after intercalation.[13] However, a capability to quantitatively image the electrochemical current of single Li-ion storage nanoparticles is yet to be demonstrated.

Here, we employ surface plasmon resonance microscopy (SPRM) to image the phase transition and Li-ion diffusion kinetics in single $LiCoO_2$ nanoparticles during electrochemical lithiation and delithiation processes. SPRM is a recently developed optical microscopy technique[14−16] to image the refractive index (RI) of individual nanoparticles themselves,[17,18] or that of the medium surrounding it.[19] It was found that the RI of single $LiCoO_2$ nanoparticles significantly decreased with the increasing delithiation state (x value in $Li_{1-x}CoO_2$), enabling an optical read-out of single nanoparticle electrochemistry. Cyclic voltammogram and charge rate were resolved for single $LiCoO_2$ nanoparticles by analyzing the SPRM images during the electrochemical cycling, from which the phase transition and Li-ion diffusion kinetics can be investigated. Imaging single nanoparticles ensured us to study the Li-ion diffusion kinetics in the absence of interparticle boundaries, leading to an intrinsic diffusion coefficient close to the theoretical prediction. Further characterization of the same region of interest with scanning electron microscopy (SEM) allowed for studying the structure−activity relationship by directly connecting the charge rate and morphology of each individual nanoparticle.

EXPERIMENTAL METHODS

Preparation and Characterizations of $LiCoO_2$ Nanoparticles. The synthesis method of $LiCoO_2$ nanoparticles was adopted from ref 20. Briefly, a mixture consisting of 1 mM lithium acetate, 1 mM cobalt(II) acetate, 20 mL of distilled water, and 2 mM citric acid anhydrous was first prepared. Subsequently, the prepared mixture was evaporated at 80 °C until formation of a polymeric resin that was further dried at 120 °C to remove the excess water. $LiCoO_2$ nanoparticles were finally obtained by grinding and calcining the remaining solid at 450 °C for 10 h. AFM (Agilent Technologies, 5500) and TEM (JEOL-2100) images were used to characterize the size of the as-synthesized $LiCoO_2$ nanoparticles. XRD was recorded by Bruker AXS D8 ADVANCE using Cu Kα radiation at 40 kV and 40 mA in the 2θ degree range from 10° to 80°. The SEM (Shimadzu, S-4800) was used to determine the morphology of single $LiCoO_2$ nanoparticles on the surface of the gold film, which was combined with SPRM to calculate the Li-ion diffusion in single $LiCoO_2$ nanoparticles.

Optical System of SPRM. The experiment was performed on home-built SPRM equipment. It was built on an inverted optical microscope (Nikon, Ti-E), on which a fiber-coupled 680 nm superluminescence diode (Qphotonics LLC, QSDM-680−2, operating power 0.2 mW), a total internal reflection fluorescence illuminator, a high numerical aperture objective (N.A. = 1.49), and a CCD camera (Pike F-032, Allied Vision Technology) were integrated. The averaged image intensity in a rectangle region of interest (ROI) was utilized to quantify the SPRM intensity of a single nanoparticle. The ROI was located at 2 μm above the nanoparticle with a size of 2.6 × 0.6 μm^2 (Supporting Information section 2). The electrochemical measurement was performed on a three-electrode potentiostat (ARFDE5, Pine Research Instrumentation). Synchronization between electrochemical measurement and CCD camera was achieved with a data acquisition card (USB-6250, National Instruments). Prior to experiment, $LiCoO_2$ nanoparticles were dispersed with ultrasonic treatment in an appropriate amount of deionized water (18.2 MΩ, Smart2Pure 3 UF, Thermo Fisher). A PDMS open chamber was placed onto the gold-coated coverslip, serving as the electrochemical cell. Subsequently, 300 μL of 1 M $LiNO_3$ electrolyte solution was added into the chamber, before an additional 20 μL aqueous solution of $LiCoO_2$ nanoparticles was injected and mixed. After 5 min, liquid was removed by pipet and thoroughly rinsed and dried. The coverslip was then baked at 60 °C for 20 min in a baking oven. Finally, 1 M $LiNO_3$ was injected into the chamber again for further optical and electrochemical measurements.

COMSOL Simulation. The SPRM image of a single $LiCoO_2$ nanoparticle with varying refractive index and geometry was numerically simulated with COMSOL multiphysics software. Surface plasmon polaritons at the interface between a gold film (thickness = 47 nm) and water were excited by a p-polarized incident plane wave (λ = 680 nm, incident angle = 70°). The refractive indices of glass, water, and gold are 1.51391, 1.331, and 0.16146 + i*3.6420, respectively. Five refractive indices were selected for the $LiCoO_2$ nanoparticle, including 2.4, 2.3, 2.2, 2.08, and 2.02. In our simulations, the geometry of

DOI: 10.1021/jacs.6b08923
J. Am. Chem. Soc. 2017, 139, 186−192

$LiCoO_2$ nanoparticle was volume-equivalently treated as a sphere-shape to avoid the sharp edge in the cylinder shape, which introduced additional difficulties to the mesh building and the finite-element calculations.

RESULTS AND DISCUSSION

SPRM Imaging of Single $LiCoO_2$ Nanoparticles. $LiCoO_2$ is one of the most successful cathode materials in commercial Li-ion batteries. $LiCoO_2$ nanoplates with layered structure were synthesized using a citrate sol−gel method[20] and systematically characterized (Supporting Information section 1). TEM and atomic force microscopy indicated that these nanosheets exhibited a layered structure with a typical size of 200 nm and a thickness of 75 nm, respectively. X-ray diffraction revealed a standard rhombohedral structure with $R\bar{3}m$ space group. For SPRM imaging, individual nanoparticles were evenly and sparsely immobilized on a gold-coated coverslip, on which planar surface plasmon resonance (SPR) was excited with an objective-based total internal reflection configuration. The detailed description of the optical setup can be found in our previous work.[14,15,19] Briefly, a low power red beam (wavelength = 680 nm, operating power = 0.2 mW) was collimated and directed into the gold-coated coverslip through the objective to generate surface plasmon polaritons at the gold−solution interface (Figure 1a).[21] The reflected light was captured by a camera to produce an SPRM image. An individual nanoparticle on the gold film was visualized in the SPRM image as it scattered the surface plasmon waves.[22−24] Any nanoparticle that was smaller than the optical diffraction limit (~500 nm in the present work) appeared as a parabolic pattern in the SPRM image as shown in the grayscale images in Figure 1a.[19,25] Although all nanoparticles exhibited similar parabolic patterns, the optical contrast was determined by the RI of the nanoparticle. Higher RI led to larger optical contrast in the SPRM image. Given the average thickness of 75 nm and the penetration depth of surface plamon wave of 200 nm, the SPRM image reflects the averaged RI of the entire $LiCoO_2$ nanoplate, rather than a bottom portion of it.

Resolving Single Nanoparticle Electrochemistry Optically. It was found that the RI of $LiCoO_2$ nanoparticles significantly decreased with increasing the delithiation state (x value in $Li_{1-x}CoO_2$), thus providing an opportunity to resolve the Li-ion extraction rate of single nanoparticles from its optical responses. In a typical cyclic voltammetry experiment, electrode potential swept between 0.3 and 0.8 V (vs Ag/AgCl) in an aqueous solution of 1 M $LiNO_3$ at a scan rate of 10 mV/s. Gold film served as both working electrode to perform electrochemistry and the optical substrate to generate SPRM images. SPR intensity of a single $LiCoO_2$ nanoparticle during cycling is displayed in Figure 1b (see Supporting Information section 2 for details). When the potential scans toward positive, Li-ions are gradually extracted from the $LiCoO_2$ nanoparticle (delithiation), accompanying a decreased SPR intensity. Oppositely, during the reversal scan, Li-ions are intercalated into the same $LiCoO_2$ nanoparticle (lithiation), leading to a complete recovery of SPR intensity. The complete recovery demonstrated the excellent reversibility of single $LiCoO_2$ nanoparticles (Supporting Information section 4). Note that while the SPRM intensity of a single nanoparticle was a function of its lithiation states, the parabolic pattern did not change within the rectangle ROI we selected (Supporting Information section 7).

The electrode current from all the nanoparticles on the gold film is shown in Figure 1c (blue curve). Three pairs of current peaks can be clearly identified, which are in good agreements with previous reports on $LiCoO_2$ electrochemistry.[26,27] The first peak (0.47/0.44 V vs Ag/AgCl) indicated the first order insulator−metal phase transition.[28] The second (0.62/0.60 V) and third (0.73/0.71 V) peaks were associated with the order−disorder transitions.[26,27] The current peaks accompanying the lithiation process were slightly broader and smaller, which was often observed in aqueous solution due to the slow desolvation process.[20,29]

Interestingly, the first order derivative of the SPR intensity curve well reproduces three pairs of phase transition peaks (red curve in Figure 1c). Note that the blue curve is the averaged electrochemical current from all of the $LiCoO_2$ nanoparticles on the electrode, and the red curve comes from the optical signal of a single nanoparticle. The similarity demonstrated the capability of SPRM to study the phase transition kinetics of single nanoparticles. Moreover, as tens of individual nanoparticles can be captured by SPRM simultaneously, the present approach enabled the high throughput recording of many nanoparticles at the same time. As examples, two videos consisting of time elapsed SPRM images of 6 and 46 $LiCoO_2$ nanoparticles were provided in Supporting Information Movies S1 and S2, respectively.

The consistency between the first derivative of SPR intensity curve and the electrochemical current indicated that SPR intensity of the $Li_{1-x}CoO_2$ nanoparticle was linearly or quasilinearly dependent on its delithiation states (x). If SPR intensity was a linear function of delithiation states (x), its first derivative (dx/dt) naturally gave the Li-ion transfer rate, which was equivalent to the electrochemical current of a single nanoparticle. In order to verify this point, a constant-current charging was performed to induce the extraction of Li-ions at a constant rate. The electrode potential curve is shown in Figure 1d (blue curve), which rapidly rises to ~0.45 V, corresponding to a delithiation state of 0.25,[26−28] and remains at this potential for ~20 s due to the insulator−metal phase transition. Further delithiation produces the second shoulder at 0.6 V (x = 0.5), and finally reaches 0.71 V (x = 0.4). The potential steps are in good agreement with literature reports[23,24] and the cyclic voltammogram in Figure 1c. Note that the galvanostatic charge curve contains both contributions from the gold electrode and $LiCoO_2$ nanoparticles, resulting in gradually slowing charging behavior (Figure S6). Accompanying the three phase transitions, three stages appeared in the SPR intensity curve of a single $LiCoO_2$ nanoparticle (red curve in Figure 1d). In stage 1, SPR intensity linearly decreases from 3000 (x = 0) to 2740 (x = 0.25) intensity unit (IU) with a factor of 10.4 IU per 0.01 delithiation state. In stage 2, the SPR intensity also linearly decreases but with a smaller factor of ~7 IU per 0.01 delithiation state. Stage 3, however, exhibits a more complicated dependence, where SPR intensity monotonically but nonlinearly decreases with delithiation states. The linear or quasilinear dependence of SPR intensity on the delithiation state provided the theoretical basis for resolving the Li-ion extraction/insertion rate of single nanoparticles from its optical response. As stage 1 exhibited the best and highest linear dependence, and it was well-documented in previous studies on the aqueous electrochemistry of $LiCoO_2$,[20,30] we focused on this transition process in the discussion below.

For the bulk electrode of $LiCoO_2$, the electrochemical lithiation is a diffusion-limited process. We demonstrated that

DOI: 10.1021/jacs.6b08923
J. Am. Chem. Soc. 2017, 139, 186−192

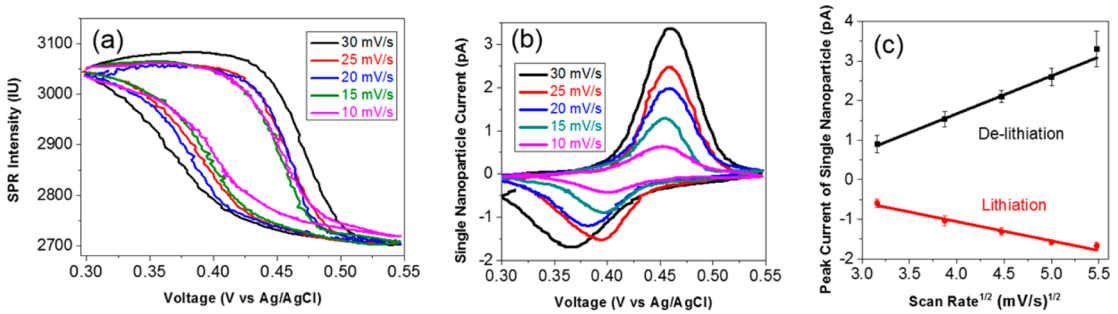

Figure 2. (a) SPR intensity curves and (b) the corresponding current, i.e., Li-ion transfer rate, of a single $LiCoO_2$ nanoparticle when sweeping potential with different scan rates. (c) The peak current of a single nanoparticle linearly increases with the square root of the increasing scan rate.

this point was still valid at the single nanoparticle level by examining the single nanoparticle voltammograms at different scan rates. Figure 2a shows the SPR intensity curves versus potential with scan rates varying from 10 to 30 mV/s. By adopting the conversion factor of ~10.4 IU per 0.01 delithiation state, the first order derivatives of these curves lead to single nanoparticle cyclic voltammograms as shown in Figure 2b (see Supporting Information section 4 for details). As shown in Figure 2c, the peak current of the single nanoparticle linearly increases with the square root of the scan rate, a clear sign of a diffusion-limited electrochemical process. Note that peak currents of a single nanoparticle as low as 0.5 pA were obtained with a good signal-to-noise ratio, demonstrating the superior sensitivity of optical recording. Thus, the spatial resolution of SPRM allowed for the simultaneous measurements of cyclic voltammograms of tens of individual $LiCoO_2$ nanoparticles, with detection sensitivity of ~50 fA for each of them.

The dependence of the refractive index of $LiCoO_2$ and its delithiation state was attributed to the enhanced electronic conductivity after the removal of Li-ions due to the high mobility of a Li vacancy. Previous experimental[31,32] and theoretical[28] studies have confirmed that the delithiation induced a Mott transition of $Li_{1-x}CoO_2$ from insulator ($x < 0.05$) to metallic ($0.05 < x < 0.5$), which was anticipated to change its dielectric constant (or refractive index) as RI was significantly affected by the electronic structure. Indeed, the direct measurement of the $Li_{1-x}CoO_2$ film revealed an RI that was highly dependent on its delithiation state.[33] The real part of RI changed between 2.4 and 2.0 when x varied from 0 to 0.5. We therefore simulated the dependence of the electric field of a surface plasmon polariton on the RI of a single $LiCoO_2$ nanoparticle with a COMSOL model we previously adopted[19] (Supporting Information section 6). Electromagnetic calculation simulated the near-field distribution of the electric field of surface plasmon polaritons (Figure 3a), which was consistent with the experimental SPRM image (Figure 3b). The simulation exhibits a 30% decrease when the RI of the nanoparticle decreases from 2.4 to 2.02, as shown in Figure 3c. This value was close to the experimental results, which decreased by 20% after electrochemical delithiation (Figure 1b). On the other hand, the delithiation of layered $LiCoO_2$ nanoplates was also known to expand its size by increasing the interlayer distance by 2.5% (from 1.4058 to 1.442 nm).[34] According to the COMSOL simulation, such volume expansion resulted in a 1.5% increase in the electric field (Figure 3c), in opposition to the experimental results.

Intrinsic Diffusion Coefficient of Li-Ion in Single Nanoparticles. In operando monitoring of the electrochemical lithiation process provided a great opportunity to determine the intrinsic diffusion coefficient of Li-ions in single $LiCoO_2$ nanoparticles by measuring the diffusion time with SPRM and characterizing the diffusion length (morphology) with SEM. An SPRM image of four individual $LiCoO_2$ nanoparticles is shown in Figure 4a. The corresponding SEM image of the same region-of-interest was obtained after the electrochemical measurements. The high resolution SEM images of each nanoparticle are also provided in Figure 4b, from which the diffusion length (L) can be estimated by calculating the equivalent diameter of cylinder geometry. SEM images reveal that $LiCoO_2$ nanoplates lay on the gold film. The direct contact between gold atoms and the *ab*-plane of the $LiCoO_2$ nanoplate was likely responsible for the electron transfer. SPRM images were collected at a frame rate of 53.4 frames per second, allowing for the study of lithiation processes as fast as tens of milliseconds. With application of a potential step from 0.3 to 0.55 V, delithiation results in a single-rate exponential decay in the SPR intensity as shown in Figure 4b. For a diffusion-limited process, Li-ion extraction kinetics was described by the following equation:[35]

$$\Delta I_{SPR}(t) = I_{SPR,0} \exp\left(-\frac{\pi^2 Dt}{4L^2}\right) \quad (1)$$

Here, the following abbreviations apply: $\Delta I_{SPR}(t)$ is the SPR intensity change as a function of time (t), $I_{SPR,0}$ is the original SPR intensity, D is the diffusion coefficient, and L is the diffusion length. By extracting the time constant (τ) with curve

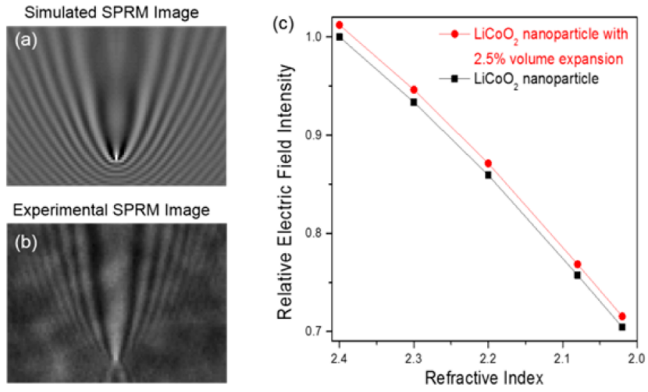

Figure 3. (a) Simulated near-field electric field distribution with a COMSOL model and (b) experimental SPRM image were consistent. (c) The relative electric field intensity decreases by 30% when the refractive index of a single nanoparticle decreases from 2.4 to 2.02. Volume expansion by 2.5% increases the relative electric field by 1.5% for all refractive indices.

DOI: 10.1021/jacs.6b08923
J. Am. Chem. Soc. 2017, 139, 186−192

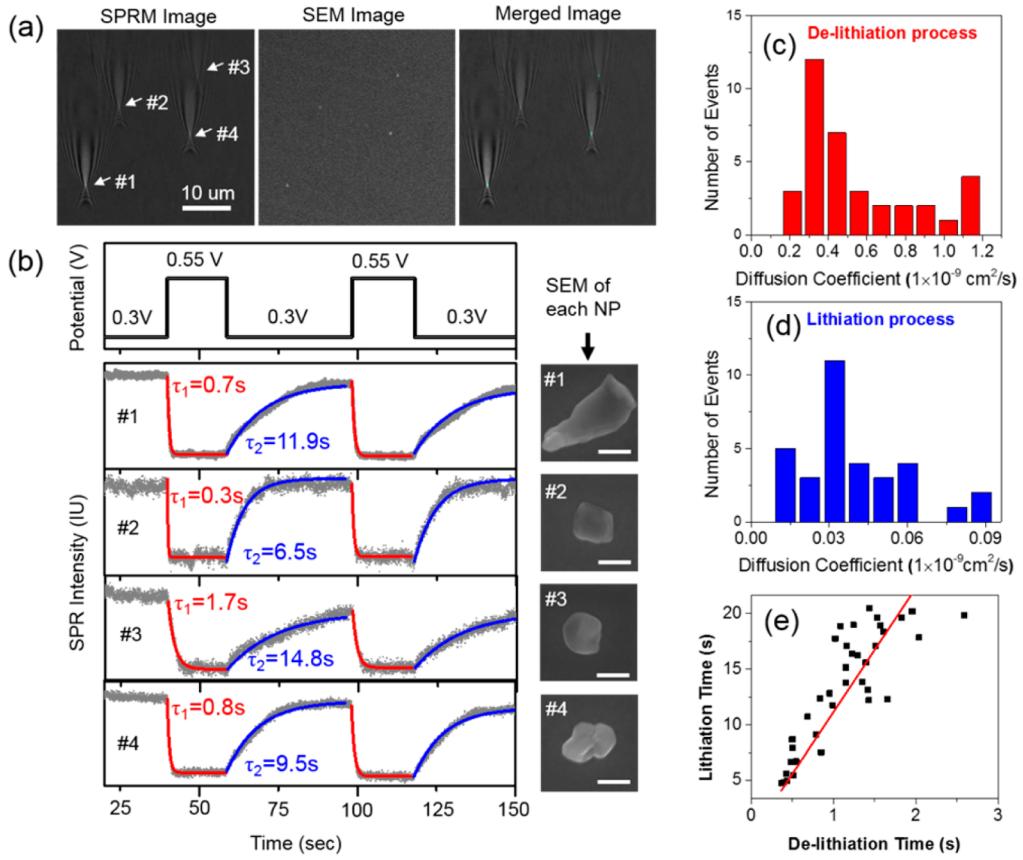

Figure 4. (a) SPRM image (left panel) and SEM image (center panel) of four $LiCoO_2$ nanoparticles are colocalized (right panel). (b) SPR intensity curves of the four $LiCoO_2$ nanoparticles when applying potential steps between 0.3 and 0.55 V. Corresponding high resolution SEM images of each nanoparticle are shown in the right side of SPR intensity curves. Scale bar: 200 nm. (c, d) Distributions of the diffusion coefficient of Li-ions in 35 single $LiCoO_2$ nanoparticles during delithiation (c) and lithiation (d) processes. (e) A clear correlation is observed between the diffusion time of single nanoparticle during delithiation and lithiation processes.

fitting, one was able to calculate the diffusion coefficient ($D = 4L^2/\pi^2\tau$) for each single nanoparticle. Interestingly, while a monoexponential function was good enough to fit the lithiation kinetics of nanoparticles with symmetrical morphology (NP #2), a biexponential function was found to better describe that of an asymmetrical nanoparticle (NP #1), implying the combination of diffusion along the long-axis and short-axis, respectively (Supporting Information Figure S14).

Diffusion coefficients of 35 individual nanoparticles exhibit a significant heterogeneity ranging from 0.2 to 1.2 × 10^{-9} cm^2/s for Li-ion extraction (Figure 4c), and from 0.01 to 0.09 × 10^{-9} cm^2/s for Li-ion insertion (Figure 4d), respectively. These values were consistent with the theoretical prediction[36,37] as well as with previous results on single grains using in situ atomic force microscopy.[38] The Li-ion insertion rates were ~10 times slower compared with the extraction rates due to the relatively slower desolvation process in aqueous solution.[20] It is worth mentioning that the diffusion coefficient was a function of delithiation states (potential).[39] In the present work, the diffusion kinetics should be considered as the overall diffusion coefficient in the entire process of a stage 1 phase transition, which was dominated by the minimal diffusion coefficient at the two-phase region around 0.47 V.

A 6-fold variation on the diffusion coefficients of single nanoparticles suggested the influence of interior crystallographic structure on the diffusion kinetics of Li-ions. Previous studies demonstrated that the diffusion coefficient was largely affected by the facet orientation,[40] lattice mismatch,[41] vacancy,[42] and stress.[43] For instance, it took 0.3 and 1.7 s for nanoparticles #2 and #3 to be delithiated, respectively, despite their similar morphologies and sizes. The imperfect crystallographic structures of as-synthesized $LiCoO_2$ nanoplates were validated by high resolution TEM. While some of the individuals displayed nearly perfect atomic alignments, others exhibited severe interior mismatches (Supporting Information Figure S3). This hypothesis was further supported by the obvious correlation between the Li-ion insertion and extraction rates for the same single nanoparticle (Figure 4e). A nanoparticle with more interior defects tended to exhibit longer diffusion time simultaneously in lithiation and delithiation processes.

CONCLUSION

In conclusion, we proposed an SPRM technique to quantitatively image the electrochemical current of single $LiCoO_2$ nanoparticles during cycling with a high sensitivity (50 fA) and fast temporal resolution (20 ms), allowing for studying the phase transition and Li-ion diffusion kinetics at single nanoparticle level. It was found that, while the intrinsic diffusion coefficient was consistent with the prediction from first principles calculations, interior crystallographic structures also played essential roles to affect the Li-ion diffusion kinetics. While existing in situ imaging technique often focused on the atomic or geometrical structures, the present work was the first

DOI: 10.1021/jacs.6b08923
J. Am. Chem. Soc. 2017, 139, 186−192

attempt to monitor the RI of single Li-ion storage nanoparticles, which exhibited several advantages. First, as RI is an intrinsic property of any material, and as it is known to be sensitive to the chemical composition and electronic structure of nanomaterials, it makes SPRM a general technique for various kinds of anode and cathode materials. This feature is particularly important for cathode materials such as transition metal oxides, as they often exhibit a very subtle volume change during lithiation. Second, SPRM can reach a fast temporal resolution up to microseconds,[44] which is thus suitable for studying fast dynamical processes from the micro- to millisecond time scale. Third, SPRM is a wide-field imaging technique and is capable of simultaneously monitoring tens of nanoparticles. The combination of SPRM with SEM and other in situ characterization techniques provides a unique capability to efficiently and appropriately establish the structure−activity relationship, which is anticipated to promote the rational design and optimization of electrode materials in a Li-ion battery.

■ ASSOCIATED CONTENT

Supporting Information

The Supporting Information is available free of charge on the ACS Publications website at DOI: 10.1021/jacs.6b08923.

Data analysis, characterization of $LiCoO_2$ nanoparticles, descriptions of movies (PDF)

Movie showing time elapsed SPRM images (AVI)

Movie showing differential SPRM images (AVI)

■ AUTHOR INFORMATION

Corresponding Author

*wei.wang@nju.edu.cn

ORCID

Dan Jiang: 0000-0001-5408-4949

Notes

The authors declare no competing financial interest.

■ ACKNOWLEDGMENTS

We acknowledge financial support from the National Natural Science Foundation of China (NSFC, Grants 21527807, 21522503, 21327008, 21327902), and the Natural Science Foundation of Jiangsu Province (BK20150013, BK20140592, BK20150570). We also thank Prof. Huigang Zhang and Prof. Zhenda Lu in Nanjing University for helpful discussion.

■ REFERENCES

(1) Sathiya, M.; Abakumov, A. M.; Foix, D.; Rousse, G.; Ramesha, K.; Saubanère, M.; Doublet, M. L.; Vezin, H.; Laisa, C. P.; Prakash, A. S.; Gonbeau, D.; VanTendeloo, G.; Tarascon, J.-M. *Nat. Mater.* **2015**, *14*, 230−238.

(2) Yoo, E.; Kim, J.; Hosono, E.; Zhou, H.-s.; Kudo, T.; Honma, I. *Nano Lett.* **2008**, *8*, 2277−2282.

(3) Zheng, G.; Lee, S. W.; Liang, Z.; Lee, H. W.; Yan, K.; Yao, H.; Wang, H.; Li, W.; Chu, S.; Cui, Y. *Nat. Nanotechnol.* **2014**, *9*, 618−623.

(4) Liu, N.; Lu, Z.; Zhao, J.; McDowell, M. T.; Lee, H.-W.; Zhao, W.; Cui, Y. *Nat. Nanotechnol.* **2014**, *9*, 187−192.

(5) Huang, J. Y.; Zhong, L.; Wang, C. M.; Sullivan, J. P.; Xu, W.; Zhang, L. Q.; Mao, S. X.; Hudak, N. S.; Liu, X. H.; Subramanian, A.; Fan, H.; Qi, L.; Kushima, A.; Li, J. *Science* **2010**, *330*, 1515−1520.

(6) Ebner, M.; Marone, F.; Stampanoni, M.; Wood, V. *Science* **2013**, *342*, 716−720.

(7) Wang, F.; Yu, H.-C.; Chen, M.-H.; Wu, L.; Pereira, N.; Thornton, K.; Van der Ven, A.; Zhu, Y.; Amatucci, G. G.; Graetz, J. *Nat. Commun.* **2012**, *3*, 1201.

(8) Liu, X. H.; Wang, J. W.; Huang, S.; Fan, F. F.; Huang, X.; Liu, Y.; Krylyuk, S.; Yoo, J.; Dayeh, S. A.; Davydov, A. V.; Mao, S. X.; Picraux, S. T.; Zhang, S.; Li, J.; Zhu, T.; Huang, J. Y. *Nat. Nanotechnol.* **2012**, *7*, 749−756.

(9) Wang, J.; Eng, C.; Chen-Wiegart, Y.-c. K.; Wang, J. *Nat. Commun.* **2015**, *6*, 7496.

(10) Fosdick, S. E.; Anderson, M. J.; Nettleton, E. G.; Crooks, R. M. *J. Am. Chem. Soc.* **2013**, *135*, 5994−5997.

(11) Li, K.; Wang, K.; Qin, W.; Deng, S.; Li, D.; Shi, J.; Huang, Q.; Fan, C. *J. Am. Chem. Soc.* **2015**, *137*, 4292−4295.

(12) Brasiliense, V.; Patel, A. N.; Martinez-Marrades, A.; Shi, J.; Chen, Y.; Combellas, C.; Tessier, G.; Kanoufi, F. *J. Am. Chem. Soc.* **2016**, *138*, 3478−3483.

(13) Bao, W.; Wan, J.; Han, X.; Cai, X.; Zhu, H.; Kim, D.; Ma, D.; Xu, Y.; Munday, J. N.; Drew, H. D.; Fuhrer, M. S.; Hu, L. *Nat. Commun.* **2014**, *5*, 4224.

(14) Wang, W.; Foley, K.; Shan, X.; Wang, S.; Eaton, S.; Nagaraj, V. J.; Wiktor, P.; Patel, U.; Tao, N. *Nat. Chem.* **2011**, *3*, 251−255.

(15) Wang, W.; Yang, Y.; Wang, S.; Nagaraj, V. J.; Liu, Q.; Wu, J.; Tao, N. *Nat. Chem.* **2012**, *4*, 846−853.

(16) Huang, B.; Yu, F.; Zare, R. N. *Anal. Chem.* **2007**, *79*, 2979−2983.

(17) Wang, S.; Shan, X.; Patel, U.; Huang, X.; Lu, J.; Li, J.; Tao, N. *Proc. Natl. Acad. Sci. U. S. A.* **2010**, *107*, 16028−16032.

(18) Fang, Y.; Wang, W.; Wo, X.; Luo, Y.; Yin, S.; Wang, Y.; Shan, X.; Tao, N. *J. Am. Chem. Soc.* **2014**, *136*, 12584−12587.

(19) Shan, X.; Díez-Pérez, I.; Wang, L.; Wiktor, P.; Gu, Y.; Zhang, L.; Wang, W.; Lu, J.; Wang, S.; Gong, Q.; Li, J.; Tao, N. *Nat. Nanotechnol.* **2012**, *7*, 668−672.

(20) Heli, H.; Yadegari, H.; Jabbari, A. *J. Appl. Electrochem.* **2012**, *42*, 279−289.

(21) Homola, J. *Chem. Rev.* **2008**, *108*, 462−493.

(22) Yu, H.; Shan, X. N.; Wang, S. P.; Chen, H. Y.; Tao, N. J. *Anal. Chem.* **2014**, *86*, 8992−8997.

(23) Demetriadou, A.; Kornyshev, A. A. *New J. Phys.* **2015**, *17*, 013041.

(24) Demetriadou, A. *Sci. Rep.* **2015**, *5*, 18247.

(25) Halpern, A. R.; Wood, J. B.; Wang, Y.; Corn, R. M. *ACS Nano* **2014**, *8*, 1022−1030.

(26) Xia, H.; Lu, L.; Meng, Y. S.; Ceder, G. *J. Electrochem. Soc.* **2007**, *154*, A337−A342.

(27) Wang, G. J.; Qu, Q. T.; Wang, B.; Shi, Y.; Tian, S.; Wu, Y. P.; Holze, R. *Electrochim. Acta* **2009**, *54*, 1199−1203.

(28) Marianetti, C. A.; Kotliar, G.; Ceder, G. *Nat. Mater.* **2004**, *3*, 627−631.

(29) Yadegari, H.; Jabbari, A.; Heli, H. *J. Solid State Electrochem.* **2012**, *16*, 227−234.

(30) Ruffo, R.; Wessells, C.; Huggins, R. A.; Cui, Y. *Electrochem. Commun.* **2009**, *11*, 247−249.

(31) Menetrier, M.; Saadoune, I.; Levasseur, S.; Delmas, C. *J. Mater. Chem.* **1999**, *9*, 1135−1140.

(32) Graetz, J.; Hightower, A.; Ahn, C. C.; Yazami, R.; Rez, P.; Fultz, B. *J. Phys. Chem. B* **2002**, *106*, 1286−1289.

(33) Rubin, M.; von Rottkay, K.; Wen, S.-J.; Özer, N.; Slack, J. *Sol. Energy Mater. Sol. Cells* **1998**, *54*, 49−57.

(34) Mukhopadhyay, A.; Sheldon, B. W. *Prog. Mater. Sci.* **2014**, *63*, 58−116.

(35) Xie, J.; Imanishi, N.; Zhang, T.; Hirano, A.; Takeda, Y.; Yamamoto, O. *Electrochim. Acta* **2009**, *54*, 4631−4637.

(36) Van der Ven, A.; Ceder, G. *Electrochem. Solid-State Lett.* **2000**, *3*, 301−304.

(37) Van der Ven, A.; Ceder, G.; Asta, M.; Tepesch, P. D. *Phys. Rev. B: Condens. Matter Mater. Phys.* **2001**, *64*, 184307.

(38) Balke, N.; Jesse, S.; Morozovska, A. N.; Eliseev, E.; Chung, D. W.; Kim, Y.; Adamczyk, L.; García, R. E.; Dudney, N.; Kalinin, S. V. *Nat. Nanotechnol.* **2010**, *5*, 749−754.

(39) Jang, Y. I.; Neudecker, B. J.; Dudney, N. J. *Electrochem. Solid-State Lett.* **2001**, *4*, A74−A77.

DOI: 10.1021/jacs.6b08923
J. Am. Chem. Soc. 2017, 139, 186−192

(40) Takeuchi, S.; Tan, H.; Bharathi, K. K.; Stafford, G. R.; Shin, J.; Yasui, S.; Takeuchi, I.; Bendersky, L. A. *ACS Appl. Mater. Interfaces* **2015**, *7*, 7901−7911.
(41) Yamakawa, S.; Yamasaki, H.; Koyama, T.; Asahi, R. *J. Power Sources* **2013**, *223*, 199−205.
(42) Moradabadi, A.; Kaghazchi, P. *Phys. Chem. Chem. Phys.* **2015**, *17*, 22917−22922.
(43) Ning, F.; Li, S.; Xu, B.; Ouyang, C. *Solid State Ionics* **2014**, *263*, 46−48.
(44) Chen, Z.; Shan, X.; Guan, Y.; Wang, S.; Zhu, J.-J.; Tao, N. *ACS Nano* **2015**, *9*, 11574−11581.

DOI: 10.1021/jacs.6b08923
J. Am. Chem. Soc. 2017, 139, 186−192